Documentation

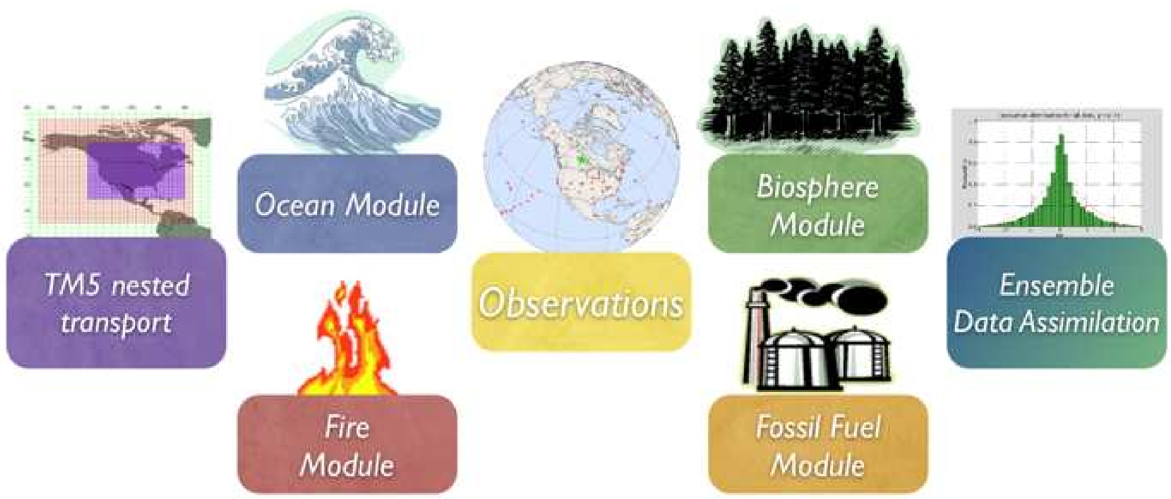

To learn more about a CarbonTracker component, click on one of the above images.
Or download the full PDF version for convenience.

Oceans Module [goto top]

1. Introduction

The oceans play an important role in the Earth's carbon cycle. They are the largest long-term sink for carbon and have an enormous capacity to store and redistribute CO_2 within the system. Oceanographers estimate that about 48% of the CO_2 from fossil fuel burning has been absorbed by the ocean [Sabine et al., 2004]. The dissolution of CO_2 in seawater shifts the balance of the ocean carbonate equilibrium towards a more acidic state (i.e., with a lower pH). This effect is already measurable [Caldeira and Wickett, 2003], and is expected to become an acute challenge to shell-forming organisms over the coming decades and centuries. Although the oceans as a whole have been a relatively steady net carbon sink, CO_2 can also come out of the oceans depending on local temperatures, biological activity, wind speeds, and ocean circulation. These processes are all considered in CarbonTracker, since they can have significant effects on the ocean sink. Improved estimates of the air-sea exchange of carbon in turn help us to understand variability of both the atmospheric burden of CO_2 and terrestrial carbon exchange.

2. Detailed Description

Oceanic uptake of CO_2 in CarbonTracker is computed using air-sea differences in partial pressure of CO_2 inferred from ocean inversions, combined with a gas transfer velocity computed from wind speeds in the atmospheric transport model.

The long-term mean air-sea fluxes, and the uncertainties associated with them, derive from the ocean interior inversions reported in Jacobson et al. [2007]. These ocean inversion flux (OIF) estimates are composed of separate preindustrial (natural) and anthropogenic flux inversions based on the methods described in Gloor et al. [2003] and biogeochemical interpretations of Gruber, Sarmiento, and Stocker [1996]. The uptake of anthropogenic CO_2 by the ocean is assumed to increase in proportion to atmospheric CO_2 levels, consistent with estimates from ocean carbon models.

For CarbonTracker 2007B, contemporary pCO_2 fields were computed by summing the preindustrial and anthropogenic flux components from inversions using five different configurations of the Princeton/GFDL MOM3 ocean general circulation model [Pacanowski and Gnanadesikan, 1998], then dividing by a gas transfer velocity computed from the European Centre for Medium-Range Weather Forecasts (ECMWF) ERA40 reanalysis. There are two small differences in first-guess fluxes in this computation from those reported in Jacobson et al. [2007]. First, the five OIF estimates all used Takahashi et al. [2002] pCO_2 estimates to provide high-resolution patterning of flux within inversion regions (the alternative "forward" model patterns were not used). To good approximation, this choice only affects the spatial and temporal distribution of flux within each of the 30 ocean inversion regions, not the magnitude of the estimated flux. Second, wind speed differences between the ERA40 product used in the offline analysis and the ECMWF operational model used in the online CarbonTracker analysis result in small deviations from the OIF estimates.

Gas transfer velocity in CarbonTracker is parameterized as a quadratic function of wind speed following Wanninkhof [1992], using the formulation for instantaneous winds. Gas exchange is computed every 3 hours using wind speeds from the ECMWF operational model as represented by the TM5 atmospheric transport model. Other than the smooth trend in anthropogenic flux assumed by the OIF results, interannual variability (IAV) in the first guess ocean flux comes entirely from wind speed effects on the gas transfer velocity. This is because the ocean inversions retrieve only a long-term mean and smooth trend.

CarbonTracker 2007A used climatogical estimates of CO_2 partial pressure in surface waters from Takahashi et al. [2002] to compute a first-guess air-sea flux. This air-sea

pCO_2 disequilibrium was modulated by a surface barometric pressure correction before being multiplied by a gas-transfer coefficient to yield a flux. In CarbonTracker 2007B, the air-sea pCO_2 disequilibrium is imposed from analysis of the OIF results, with short-term flux variability derived from the atmospheric model wind speeds via the gas transfer coefficient. The barometric pressure correction has been removed so that climatological high- and low-pressure cells do not bias the long-term means of the first guess fluxes. In either method, the first-guess fluxes have no interannual variability (IAV) due to pCO_2 changes, such as those that occur in the tropical eastern Pacific during an El Niño. In CarbonTracker, this flux IAV must be inferred from atmospheric CO_2 signals.

Air-sea transfer is inhibited by the presence of sea ice, and for this work fluxes are scaled by the daily sea ice fraction in each gridbox provided by the ECMWF forecast data.

The first-guess fluxes described here are subject to scaling during the CarbonTracker optimization process, in which atmospheric CO_2 mole fraction observations are combined with transport simulated by the atmospheric model to infer flux signals. In this process, signals of terrestrial flux in atmospheric CO_2 distribution can be erroneously interpreted as being caused by oceanic fluxes. This flux "aliasing" or "leakage" is evident in some regions as a change in the shape of the seasonal cycle of air-sea flux. Differences between CT2007B posterior air-sea fluxes and those of the OIF prior fluxes are minor, but do constitute an issue that we will be investigating in the future.

3. Further Reading

- NOAA Pacific Marine Environmental Laboratory (PMEL)
- Ocean Acidification
- Caldeira, K., and M. E. Wickett (2003), Anthropogenic carbon and ocean pH, Nature, 425365-365.
- Gloor, M., N. Gruber, J. Sarmiento, C. L. Sabine, R. A. Feely, and C. Röbeck (2003), A first estimate of present and preindustrial air-sea CO_2 flux patterns based on ocean interior carbon measurements and models, Geophysical Research Letters, 30, , 10.1029/2002GL015594.
- Gruber, N., J. L. Sarmiento, and T. F. Stocker (1996), An improved method for detecting anthropogenic CO_2 in the oceans, Global Biogeochemical Cycles, 10, , 809-837.
- Jacobson, A. R., N. Gruber, J. L. Sarmiento, M. Gloor, and S. E. Mikaloff Fletcher (2007), A joint atmosphere-ocean inversion for surface fluxes of carbon dioxide: I. Methods and global-scale fluxes, Global Biogeochemical Cycles, 21, doi:10.1029/2005GB002556.
- Pacanowski, R. C., and A. Gnanadesikan (1998), Transient response in a z-level ocean model that resolves topography with partial cells, Monthly Weather

Review, 126, 3248--3270.

- Sabine, C. L., R. A. Feely, N. Gruber, R. M. Key, K. Lee, J. L. Bullister, R. Wanninkhof, C. S. Wong, D. W. R. Wallace, B. Tilbrook, F. J. Millero, T. H. Peng, A. Kozyr, T. Ono, and A. F. Rios (2004), The oceanic sink for anthropogenic CO_2, Science, 305, 367-371.
- Takahashi, T., S. C. Sutherland, C. Sweeney, A. P. N. Metzl, B. Tilbrook, N. Bates, R. Wanninkhof, R. A. Feely, C. Sabine, J. Olafsson, and Y. Nojiri (2002), Global air-sea CO_2 flux based on climatological surface ocean pCO_2, and seasonal biological and temperature effects, Deep-Sea Research II, 49, , 1601--1622.
- Wanninkhof, R. (1992), Relationship between wind speed and gas exchange over the ocean, Journal of Geophysical Research, 97, 7373--7382.

Biosphere Module [goto top]

1. Introduction

The biospheric component of the carbon cycle consists of all the carbon stored in 'biomass' around us. This includes trees, shrubs, grasses, carbon within soils, dead wood, and leaf litter. Such reservoirs of carbon can exchange CO_2 with the atmosphere. Exchange starts when plants take up CO_2 during their growing season through the process called photosynthesis (uptake). Most of this carbon is released back to the atmosphere throughout the year through a process called respiration (release). This includes both the decay of dead wood and litter and the metabolic respiration of living plants. Of course, plants can also return carbon to the atmosphere when they burn, as described here. Even though the yearly sum of uptake and release of carbon amounts to a relatively small number (a few petagrams (one Pg=10^{15} g)) of carbon per year, the flow of carbon each way is as large as 120 Pg each year. This is why the net result of these flows needs to be monitored in a system such as ours. It is also the reason we need a good physical description (model) of these flows of carbon. After all, from the atmospheric measurements we can only see the small net sum of the large two-way streams (gross fluxes). Information on what the biospheric fluxes are doing in each season, and in every location on Earth is derived from a specialized biosphere model, and fed into our system as a first guess, to be refined by our assimilation procedure.

2. Detailed Description

The biosphere model currently used in CarbonTracker is the Carnegie-Ames Stanford Approach (CASA) biogeochemical model. This model calculates global carbon fluxes using input from weather models to drive biophysical processes, as well as satellite observed Normalized Difference Vegetation Index (NDVI) to track plant phenology. The version of CASA model output used so far was driven by year specific weather and satellite observations, and including the effects of fires on photosynthesis and respiration (see van der Werf et al., [2006] and Giglio et al., [2006]). This simulation gives 1x1 degree global fluxes on a monthly time resolution.

Net Ecosystem Exchange (NEE) is re-created from the monthly mean CASA Net Primary Production (NPP) and ecosystem respiration (R_E). Higher frequency variations (diurnal, synoptic) are added to Gross Primary Production (GPP=2*NPP) and R_E(=NEE-GPP) fluxes every 3 hours using a simple temperature Q_{10} relationship assuming a global Q_{10} value of 1.5 for respiration, and a linear scaling of photosynthesis with solar radiation. The procedure is very similar, but **NOT** identical to the procedure in Olsen and Randerson [2004] and based on ECMWF analyzed meteorology. Note that the introduction of 3-hourly variability conserves the monthly mean NEE from the CASA model. Instantaneous NEE for each 3-hour interval is thus created as:

$$NEE(t) = GPP(I, t) + R_E(T, t)$$

$$GPP(t) = I(t) * (\Sigma(GPP) / \Sigma(I))$$

$$R_E(t) = Q_{10}(t) * (\Sigma(R_E) / \Sigma(Q_{10}))$$

$$Q_{10}(t) = 1.5^{((T_{2m}-T_0) / 10.0)}$$

where T=2 meter temperature, I=incoming solar radiation, t=time, and summations are done over one month in time, per gridbox. The instantaneous fluxes yielded realistic diurnal cycles when used in the TransCom Continuous experiment.

The current CarbonTracker 2007B release was based on the CASA runs for the GFED2 project to estimate fire emissions. We found a significantly better match to observations when using this output compared to the fluxes from a neutral biosphere simulation. Due to the inclusion of fires, inter-annual variability in weather and NDVI, the fluxes for North America start with a small net flux even when no assimilation is done. This flux ranges from 0.05 PgC/yr of release, to 0.15 PgC/yr of uptake.

3. Further Reading

- CASA with fires model overview
- CASA results from Jim Randerson
- GFED2 results from Guido van der Werf, Jim Randerson, and colleagues
- Olsen and Randerson, paper
- Giglio et al., 2006 paper
- van der Werf et al., 2006 paper

Fire Module [goto top]

1. Introduction

Vegetation fires are an important part of the carbon cycle and have been so for many millennia. Even before human civilization began to use fires to clear land for agricultural purposes, most ecosystems were subject to natural wildfires that would rejuvenate old forests and bring important minerals to the soils. When fires consume part of the landscape in either controlled or natural burning, carbon dioxide (amongst many other gases and aerosols) is released in large quantities. Each year, vegetation fires emit more than 2 PgC as CO_2 into the atmosphere, mostly in the tropics. Nowadays, a large fraction of these fires is started by humans, and mostly intentionally to clear land for agriculture, or to re-fertilize soils before a new growing season. This important component of the carbon cycle is monitored mostly from space, while sophisticated 'biomass burning' models are used to estimate the amount of CO_2 emitted by each fire. Such estimates are then used in CarbonTracker to prescribe the emissions, without further refinement by our measurements.

2. Detailed Description

The fire module currently used in CarbonTracker is based on the Global Emissions Fire Database version 2 (GFEDv2), which is derived from the CASA biogeochemical model as described here. The dataset consists of 1x1 degree gridded monthly burned area, fuel loads, combustion completeness, and fire emissions (Carbon, CO_2, CO, CH_4, NMHC, H_2, NO_x, N_2O, PM2.5, Total Particulate Matter, Total Carbon, Organic Carbon, Black Carbon) for the time period spanning January 1997 - December 2006, of which we currently only use CO_2. The GFEDv2 burned area is based on MODIS satellite observations of fire counts. These, together with detailed vegetation cover information and a set of vegetation specific scaling factors, allow predictions of burned area over the time span that active fire counts from MODIS are available. The relationship between fire counts and burned area is derived, for the specific vegetation types, from a 'calibration' subset of 500m resolution burned area from MODIS in the period 2001-2004.

Once burned area has been estimated globally, emissions of trace gases are calculated using the CASA biosphere model. The seasonally changing vegetation and soil biomass stocks in the CASA model are combusted based on the burned area estimate, and converted to atmospheric trace gases using estimates of fuel loads, combustion completeness, and burning efficiency.

GFEDv2 products were successfully used in recent studies of CH_4, CO_2, CO, and other trace gases.

3. Further Reading

- CASA with fires model overview

- CASA results from Jim Randerson
- GFED2 results from Guido van der Werf, Jim Randerson, and colleagues
- Giglio et al., 2006 paper
- Interannual variability in global biomass burning emissions from 1997 to 2004. ATMOSPHERIC CHEMISTRY AND PHYSICS 6: 3423-3441 AUG 21 2006

Observations [goto top]

1. Introduction

The observations of CO_2 mole fraction by NOAA ESRL and partner laboratories are at the heart of CarbonTracker. They inform us on changes in the carbon cycle, whether they are regular (such as the seasonal growth and decay of leaves and trees), or irregular (such as the release of tons of carbon by a wildfire). The results in CarbonTracker depend directly on the quality and amount of observations available, and the degree of detail at which we can monitor the carbon cycle reliably increases strongly with the density of our observing network.

2. Detailed Description

This study uses all analyzed air samples taken at the surface from the NOAA ESRL Cooperative Air Sampling Network available for each year studied, except those flagged for analysis or sampling problems, or those thought to be influenced by local sources. The composition of the network thus varies per week depending on successful sampling and analysis, and each site's sampling frequency. In addition, we use in situ quasi-continuous CO_2 time series from seven towers: (1) the 396m level of the WLEF tower in Wisconsin; (2) the 107m level of the AMT tower in Argyle, Maine; (3) the 251m level of the KWKT tower in Texas; (4) the 40m level of the tower in Fraserdale, Canada operated by Environment Canada (EC); (5) the 23m level of the tower at Candle Lake (formerly Old Black Spruce), Canada operated by EC; (6) the 9m level of the tower at Storm Peak Laboratory operated by NCAR; and (7) the 5m level of the tower at Niwot Ridge operated by NCAR. Other in situ quasi-continuous CO_2 time series used are from the NOAA ESRL observatories at Barrow, Mauna Loa, Samoa, and South Pole, and the EC programs at Alert, Canada and Sable Island, Canada. Note that all of these observations are calibrated against the same world CO_2 standard (WMO-2005). Also, note that aircraft observations from the NOAA ESRL program were NOT assimilated, but used for independent assessment of the CarbonTracker results.

At the tower-based quasi-continuous sampling sites, we construct one daytime average (12:00-16:00 Local Standard Time) mole fraction for each day from the time series, recognizing that our atmospheric transport model does not always capture the continental nighttime stability regime while daytime well-mixed conditions are better matched. At mountain-top sites (MLO, NWR, and SPL), we use midnight-4:00 LST averages as this tends to be the most stable time period and avoids periods of upslope flows that contain local vegetative and/or anthropogenic influence. Moreover, observations at sub-daily time scales are likely to be strongly correlated and therefore add relatively little independent information to our results. Also based on Transcom continuous simulations, we decided to move a set of coastal sites by one degree into the ocean to force the model sample to be more representative of the actual site conditions. These sites are labeled for reference in the complete table of sites used in CarbonTracker.

We apply a further selection criterion during the assimilation to exclude non-Marine Boundary Layer (MBL) observations that are very poorly forecasted in our framework. We use the so-called model-data mismatch in this process, which is the random error ascribed to each observation to account for measurement errors as well as modeling errors of that observation. We interpret an observed-minus-forecasted (OmF) mole fraction that exceeds 3 times the prescribed model-data mismatch as an indicator that our modeling framework fails. This can happen for instance when an air sample is representative of local exchange not captured well by our 1x1 degree fluxes, when local meteorological conditions are not captured by our offline transport fields, but also when large-scale CO_2 exchange is suddenly changed (e.g. fires, pests, droughts) to an extent that can not be accommodated by our flux modules. This last situation would imply an important change in the carbon cycle and has to be recognized by the researchers when analyzing the results. In accordance with the 3-sigma rejection criterion, ~2% of the observations are discarded through this mechanism in our assimilations. Table 1 gives a summary of the observing sites used in CarbonTracker and the assimilation performance.

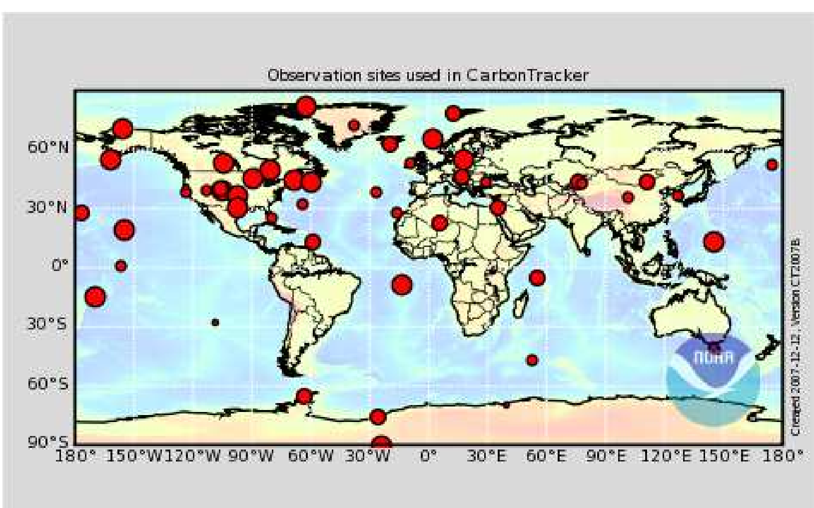

Code	Name	Lat, Lon,	Lab	N	N	mismatch	Inn X2

		Elev		used	flagged		
alt_06c0	Alert, Nunavut, Canada	82 27'N, 62 31'W, 200.0m	EC	2347	0	2.50	0.20
amt_01c3	Argyle, Maine, United States	45 2'N, 68 41'W, 50.0m	ESRL	996	8	3.00	0.67
brw_01c0	Barrow, Alaska, United States	71 19'N, 156 36'W, 11.0m	ESRL	1951	1	2.50	0.31
cdl_06c3	Candle Lake, Saskatchewan, Canada	53 59'N, 105 7'W, 628.0m	EC	1388	4	3.00	0.65
frd_06c3	Fraserdale, Canada	49 53'N, 81 34'W, 210.0m	EC	2321	11	3.00	0.51
lef_01c3	Park Falls, Wisconsin, United States	45 56'N, 90 16'W, 472.0m	ESRL	2116	11	3.00	0.61
mlo_01c0	Mauna Loa, Hawaii, United States	19 32'N, 155 35'W, 3397.0m	ESRL	1260	0	0.75	0.82
nwr_03c3	Niwot Ridge, Colorado, United States	40 3'N, 105 35'W, 3523.0m	NCAR	395	0	3.00	0.26
sbl_06c3	Sable Island, Nova Scotia, Canada	43 56'N, 60 1'W, 5.0m	EC	1180	11	3.00	0.47
smo_01c0	Tutuila, American Samoa	14 14'S, 170 34'W, 42.0m	ESRL	2206	0	0.75	1451.49
spl_03c3	Storm Peak Laboratory (Desert Research Institute), United States	40 27'N, 106 44'W, 3210.0m	NCAR	470	0	3.00	0.39
spo_01c0	South Pole, Antarctica, United States	89 59'S, 24 48'W, 2810.0m	ESRL	2440	0	0.75	0.27
wkt_01c3	Moody, Texas, United States	31 19'N, 97 20'W, 251.0m	ESRL	859	8	3.00	0.72
alt_01d0	Alert, Nunavut, Canada	82 27'N, 62 31'W, 200.0m	ESRL	334	0	1.50	0.46
asc_01d0	Ascension Island, United Kingdom	7 55'S, 14 25'W, 54.0m	ESRL	594	0	0.75	1.09
ask_01d0	Assekrem, Algeria	23 11'N, 5 25'E, 2728.0m	ESRL	306	0	1.50	0.40
azr_01d0	Terceira Island, Azores, Portugal	38 46'N, 27 23'W, 40.0m	ESRL	223	4	1.50	0.94
bal_01d0	Baltic Sea, Poland	55 21'N, 17 13'E, 3.0m	ESRL	549	0	7.50	0.43
bkt_01d0	Bukit Kototabang, Indonesia	0 12'S, 100 19'E, 864.5m	ESRL	106	0	7.50	0.67

bme_01d0	St. Davids Head, Bermuda, United Kingdom	32 22'N, 64 39'W, 30.0m	ESRL	207	8	1.50	1.27
bmw_01d0	Tudor Hill, Bermuda, United Kingdom	32 16'N, 64 53'W, 30.0m	ESRL	236	2	1.50	1.04
brw_01d0	Barrow, Alaska, United States	71 19'N, 156 36'W, 11.0m	ESRL	315	2	1.50	0.72
bsc_01d0	Black Sea, Constanta, Romania	44 10'N, 28 41'E, 3.0m	ESRL	268	1	7.50	0.75
cba_01d0	Cold Bay, Alaska, United States	55 12'N, 162 43'W, 25.0m	ESRL	530	23	1.50	1.26
cgo_01d0	Cape Grim, Tasmania, Australia	40 41'S, 144 41'E, 94.0m	ESRL	286	0	1.50	0.10
chr_01d0	Christmas Island, Republic of Kiribati	1 42'N, 157 10'W, 3.0m	ESRL	265	0	0.75	1.72
crz_01d0	Crozet Island, France	46 27'S, 51 51'E, 120.0m	ESRL	229	0	0.75	0.36
eic_01d0	Easter Island, Chile	27 9'S, 109 27'W, 50.0m	ESRL	163	0	7.50	0.03
gmi_01d0	Mariana Islands, Guam	13 26'N, 144 47'E, 1.0m	ESRL	533	0	1.50	0.40
hba_01d0	Halley Station, Antarctica, United Kingdom	75 35'S, 26 30'W, 30.0m	ESRL	327	0	0.75	0.31
hun_01d0	Hegyhatsal, Hungary	46 57'N, 16 39'E, 248.0m	ESRL	322	1	7.50	0.45
ice_01d0	Storhofdi, Vestmannaeyjar, Iceland	63 20'N, 20 17'W, 118.0m	ESRL	308	1	1.50	0.51
izo_01d0	Tenerife, Canary Islands, Spain	28 18'N, 16 29'W, 2360.0m	ESRL	247	2	1.50	1.07
key_01d0	Key Biscayne, Florida, United States	25 40'N, 80 12'W, 3.0m	ESRL	227	0	2.50	0.34
kum_01d0	Cape Kumukahi, Hawaii, United States	19 31'N, 154 49'W, 3.0m	ESRL	314	0	1.50	0.41
kzd_01d0	Sary Taukum, Kazakhstan	44 27'N, 75 34'E, 412.0m	ESRL	322	1	2.50	0.98
kzm_01d0	Plateau Assy, Kazakhstan	43 15'N, 77 53'E, 2519.0m	ESRL	283	1	2.50	1.22
mhd_01d0	Mace Head, County Galway, Ireland	53 20'N, 9 54'W, 25.0m	ESRL	265	0	2.50	0.22
mid_01d0	Sand Island, Midway, United States	28 13'N, 177 23'W, 3.7m	ESRL	311	0	1.50	0.65

mkn_01d0	Mt. Kenya, Kenya	0 3'S, 37 18'E, 3897.0m	ESRL	75	0	2.50	1.04
mlo_01d0	Mauna Loa, Hawaii, United States	19 32'N, 155 35'W, 3397.0m	ESRL	363	0	1.50	0.24
nmb_01d0	Gobabeb, Namibia	23 35'S, 15 2'E, 456.0m	ESRL	20	0	2.50	0.15
nwr_01d0	Niwot Ridge, Colorado, United States	40 3'N, 105 35'W, 3523.0m	ESRL	310	1	1.50	0.82
obn_01d0	Obninsk, Russia	55 7'N, 36 36'E, 183.0m	ESRL	88	0	7.50	0.38
oxk_01d0	Ochsenkopf, Germany	50 4'N, 11 48'E, 1193.0m	ESRL	42	4	2.50	1.29
pal_01d0	Pallas-Sammaltunturi, GAW Station, Finland	67 58'N, 24 7'E, 560.0m	ESRL	187	2	2.50	0.79
poc_01d1	Pacific Ocean, N/A	99 59'S, 999 59'W, 10.0m	ESRL	1415	0	7.50	0.03
psa_01d0	Palmer Station, Antarctica, United States	64 55'S, 64 0'W, 10.0m	ESRL	328	0	0.75	0.53
pta_01d0	Point Arena, California, United States	38 57'N, 123 44'W, 17.0m	ESRL	212	0	7.50	0.37
rpb_01d0	Ragged Point, Barbados	13 10'N, 59 26'W, 45.0m	ESRL	317	0	1.50	0.83
sey_01d0	Mahe Island, Seychelles	4 40'S, 55 10'E, 3.0m	ESRL	304	0	0.75	1.08
sgp_01d0	Southern Great Plains, Oklahoma, United States	36 48'N, 97 30'W, 314.0m	ESRL	530	9	2.50	0.84
shm_01d0	Shemya Island, Alaska, United States	52 43'N, 174 6'E, 40.0m	ESRL	253	2	2.50	0.78
smo_01d0	Tutuila, American Samoa	14 14'S, 170 34'W, 42.0m	ESRL	369	0	1.50	0.17
spo_01d0	South Pole, Antarctica, United States	89 59'S, 24 48'W, 2810.0m	ESRL	344	0	1.50	0.05
stm_01d0	Ocean Station M, Norway	66 0'N, 2 0'E, 0.0m	ESRL	597	1	1.50	0.76
sum_01d0	Summit, Greenland	72 35'N, 38 29'W, 3238.0m	ESRL	231	0	1.50	0.47
syo_01d0	Syowa Station, Antarctica, Japan	69 0'S, 39 35'E, 11.0m	ESRL	163	0	0.75	0.55

tap_01d0	Tae-ahn Peninsula, Republic of Korea	36 44'N, 126 8'E, 20.0m	ESRL	233	1	7.50	0.55
tdf_01d0	Tierra Del Fuego, Ushuaia, Argentina	54 52'S, 68 29'W, 20.0m	ESRL	90	0	0.75	0.44
thd_01d0	Trinidad Head, California, United States	41 3'N, 124 9'W, 107.0m	ESRL	184	19	2.50	1.55
uta_01d0	Wendover, Utah, United States	39 54'N, 113 43'W, 1320.0m	ESRL	293	1	2.50	0.31
uum_01d0	Ulaan Uul, Mongolia	44 27'N, 111 6'E, 914.0m	ESRL	320	0	2.50	0.73
wis_01d0	Sede Boker, Negev Desert, Israel	31 8'N, 34 53'E, 400.0m	ESRL	342	1	2.50	0.73
wlg_01d0	Mt. Waliguan, Peoples Republic of China	36 17'N, 100 54'E, 3810.0m	ESRL	215	5	1.50	1.10
zep_01d0	Ny-Alesund, Svalbard, Norway and Sweden	78 54'N, 11 53'E, 475.0m	ESRL	399	2	1.50	0.79
all	Total			36223	148	0.00	87.57

3. Further Reading

- ESRL Carbon Cycle Program
- WMO/GAW Report No. 168, 2006

Fossil Fuel Module [goto top]

1. Introduction

Human beings first influenced the carbon cycle through land-use change. Early humans used fire to control animals and later cleared forest for agriculture. Over the last two centuries, following the industrial and technical revolutions and the world population increase, fossil fuel combustion has become the largest anthropogenic source of CO_2. Coal, oil and natural gas combustion indeed are the most common energy sources in both developed and developing countries. Various sectors of the economy rely on fossil fuel combustion: power generation, transportation, residential/commercial building heating, and industrial processes. In 2004, the world emissions of CO_2 from fossil fuel burning, cement manufacturing, and flaring reached 7.9 PgC (one PgC=10^{15} grams of carbon) [CDIAC] and we estimate the global total for 2006 to be 8.4 PgC. This represents a 36% increase over 1990. The North American (U.S.A, Canada, and Mexico) flux of CO_2 to the atmosphere from fossil fuel burning was 1.9 PgC in 2004, representing 23% of the global total. The International Energy Outlook has projected that the global total source will reach 9.2 PgC in 2015 and 11.9 PgC in 2030 [DOE]. Recently, however, fossil fuel emissions have accelerated significantly, and we are now on track to exceed this 2015 projection sometime in 2008.

2. Detailed Description

The fossil fuel emission inventory used in CarbonTracker is derived from independent global total and spatially-resolved inventories. Annual global total fossil fuel CO_2 emissions are from the Carbon Dioxide Information and Analysis Center (CDIAC) [Marland et al. 2006] which extend through 2004. Fluxes are then spatially distributed in two steps: First, we use the country totals from Marland et al. [2006] for the coarse scale flux distribution, and then we distribute the country totals within the countries according to the spatial patterns from the EDGAR inventories [EDGAR, Olivier and Berdowski, 2001]. In order to extrapolate these fluxes to 2005 and 2006, we derive relative increases for each fuel type (solid, liquid and gas) and for each country from the BP Statistical Review of World Energy Statistics for 2005 and 2006. The CDIAC country-by-country totals, however, do not sum to the CDIAC global total. We hold the global totals to be more accurate and ascribe the difference (about 0.3 PgC/yr) to marine bunker fuels. Emissions from these bunker fuels are placed entirely in the ocean basins along shipping routes according to patterns from the EDGAR database. Finally, a seasonal cycle based on the Blasing et al. [2005] analysis for the United States, which has ~20% higher emissions in winter than in summer, is imposed on the North American emissions between 30 and 60 degrees north; at the present time, no seasonality is imposed on emissions outside North America. The uncertainty attached to the total source is of the order of 15%. This source is not optimized in the current CarbonTracker system as we do not believe our current network can constrain this source separately from the others. Although the contribution of CO_2 from fossil fuel burning to the observed CO_2 mole fraction is considered known, extra model error is included in the system to represent the random errors in fossil fuels.

3. Further Reading

- CDIAC (Marland et al.) Annual Global and National fluxes
- Energy Information Administration (EIA)
- BP Statistical review of World Energy
- EDGAR Database
- CDIAC (Blasing et al.) Monthly USA fluxes

TM5 Nested Transport [goto top]

1. Introduction

The link between observations of CO_2 in the atmosphere and the exchange of CO_2 at the Earth's surface is transport in the atmosphere: storm systems, cloud complexes, and weather of all sorts cause winds that transport CO_2 around the world. As a result, local events like fires, forest growth, and ocean upwelling can have impacts at remote locations. To simulate the winds and the weather, CarbonTracker uses sophisticated numerical models that are driven by the daily weather forecasts from the specialized meteorological centers of the world. Since CO_2 does not decay or react in the lower atmosphere, the influence of emissions and uptake in locations such as North America and Europe are ultimately seen in our measurements even at the South Pole! Getting the transport of CO_2 just right is an enormous challenge, and costs us almost 90% of the computer resources for CarbonTracker. To represent the atmospheric transport, we use the Transport Model 5 (TM5). This is a community-supported model whose development is shared among many scientific groups with different areas of expertise. TM5 is used for many applications other than CarbonTracker, including forecasting air-quality, studying the dispersion of aerosols in the tropics, tracking biomass burning plumes, and predicting pollution levels that future generations might have to deal with.

2. Detailed Description

TM5 is a global model with two-way nested grids; regions for which high-resolution simulations are desired can be nested in a coarser grid spanning the global domain. The advantage to this approach is that transport simulations can be performed with a regional focus without the need for boundary conditions from other models. Further, this approach allows measurements outside the "zoom" domain to constrain regional fluxes in the data assimilation, and ensures that regional estimates are consistent with global constraints. TM5 is based on the predecessor model TM3, with improvements in the advection scheme, vertical diffusion parameterization, and meteorological preprocessing of the wind fields (Krol et al., 2005). The model is developed and maintained jointly by the Institute for Marine and Atmospheric Research Utrecht (IMAU, The Netherlands), the Joint Research Centre (JRC, Italy), the Royal Netherlands Meteorological Institute (KNMI, The Netherlands), and NOAA ESRL (USA). In CarbonTracker, TM5 separately simulates advection, convection (deep and shallow), and vertical diffusion in the planetary boundary layer and free troposphere.

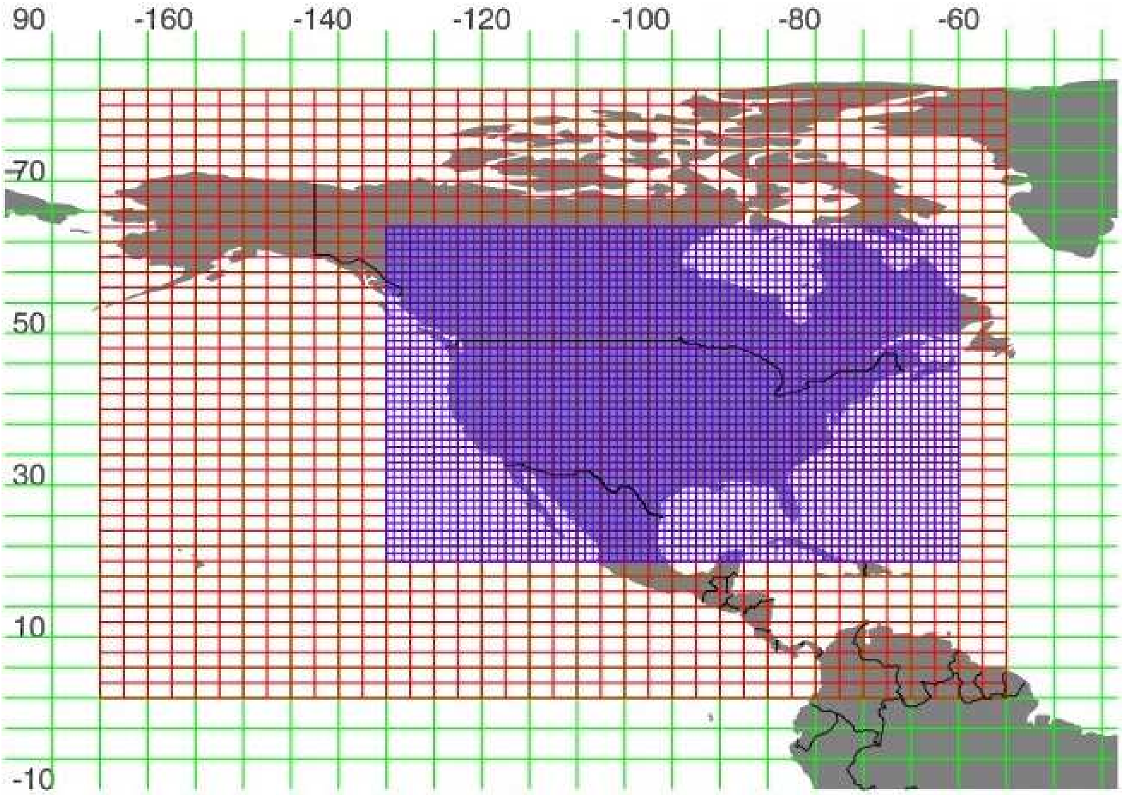

The winds which drive TM5 come from the European Center for Medium range Weather Forecast (ECMWF) operational forecast model. This "parent" model currently runs with ~25 km horizontal resolution and 60 layers in the vertical prior to 2006 (and 91 layers layers in the vertical from 2006 onwards). The carbon dioxide levels predicted by CarbonTracker do not feed back onto these predictions of winds.

For use in TM5, the ECMWF meteorological data are preprocessed into coarser grids. In CarbonTracker, TM5 is run at a global 6x4 degrees resolution with nested regions over North America (3x2 degrees) and the United States (1x1 degree) similar to the set-up in Peters et al., [2004, 2005]. The grid over North America is shown in the figure. TM5 runs at an external time step of three hours, but due to the symmetrical operator splitting and the refined resolution in nested grids, processes at the finest scale are repeated every 10 minutes. The vertical resolution of TM5 in CarbonTracker is 25 hybrid sigma-pressure levels, unevenly spaced with more levels near the surface. Approximate heights of the mid-levels (in meters, with a surface pressure of 1012 hPa) are:

Level	Height (m)	Level	Height (m)
1	34.5	14	9076.6
2	111.9	15	10533.3
3	256.9	16	12108.3
4	490.4	17	13874.2

5	826.4	18	15860.1
6	1274.1	19	18093.2
7	1839.0	20	20590.0
8	2524.0	21	24247.3
9	3329.9	22	29859.6
10	4255.6	23	35695.0
11	5298.5	24	42551.5
12	6453.8	25	80000.0
13	7715.4		

3. Further Reading

- The TM5 model homepage
- ECMWF forecast model technical documentation
- The NCEP reanalysis meteo data
- Peters et al., 2004, JGR paper on transport in TM5
- Krol et al., 2005, ACP overview paper of the TM5 model

Ensemble Data Assimilation [goto top]

1. Introduction

Data assimilation is the name of a process by which observations of the 'state' of a system help to constrain the behavior of the system in time. An example of one of the earliest applications of data assimilation is the system in which the trajectory of a flying rocket is constantly (and rapidly) adjusted based on information of its current position to guide it to its exact final destination. Another example of data assimilation is a weather model that gets updated every few hours with measurements of temperature and other variables, to improve the accuracy of its forecast for the next day, and the next, and the next. Data assimilation is usually a cyclical process, as estimates get refined over time as more observations about the "truth" become available. Mathematically, data assimilation can be done with any number of techniques. For large systems, so-called variational and ensemble techniques have gained most popularity. Because of the size and complexity of the systems studied in most fields, data assimilation projects inevitably include supercomputers that model the known physics of a system. Success in guiding these models in time often depends strongly on the number of observations available to inform on the true system state.

In CarbonTracker, the model that describes the system contains relatively simple descriptions of biospheric and oceanic CO_2 exchange, as well as fossil fuel and fire emissions. In time, we alter the behavior of this model by adjusting a small set of parameters as described in the next section.

2. Detailed Description

The four surface flux modules drive instantaneous CO_2 fluxes in CarbonTracker according to:

$$F(x, y, t) = \lambda \bullet F_{bio}(x, y, t) + \lambda \bullet F_{oce}(x, y, t) + F_{ff}(x, y, t) + F_{fire}(x, y, t)$$

Where λ represents a set of linear scaling factors applied to the fluxes, to be estimated in the assimilation. These scaling factors are the final product of our assimilation and together with the modules determine the fluxes we present in CarbonTracker. Note that no scaling factors are applied to the fossil fuel and fire modules.

2.1 Land-surface classification

The scaling factors λ are estimated for each week and assumed constant over this period. Each scaling factor is associated with a particular region of the global domain, and currently the geographical distribution of the regions is fixed. The choice of regions is a strong *a-priori* constraint on the resulting fluxes and should be approached with care to avoid so-called "aggregation errors" [Kaminsky, 1999]. We chose an approach in which the ocean is divided up into 11 large basins encompassing large-scale ocean circulation features, as in the TransCom inversion study (e.g. Gurney et al., [2002]). The terrestrial biosphere is divided up according to ecosystem type as well as geographical location. Thereto, each of the 11 TransCom land regions contains a maximum of 19 ecosystem types summarized in the table below. The figure shows ecoregions for North America (click here for global land ecoregions). Note that there is currently no requirement for ecoregions to be contiguous, and a single scaling factor can be applied to the same vegetation type on both sides of a continent.

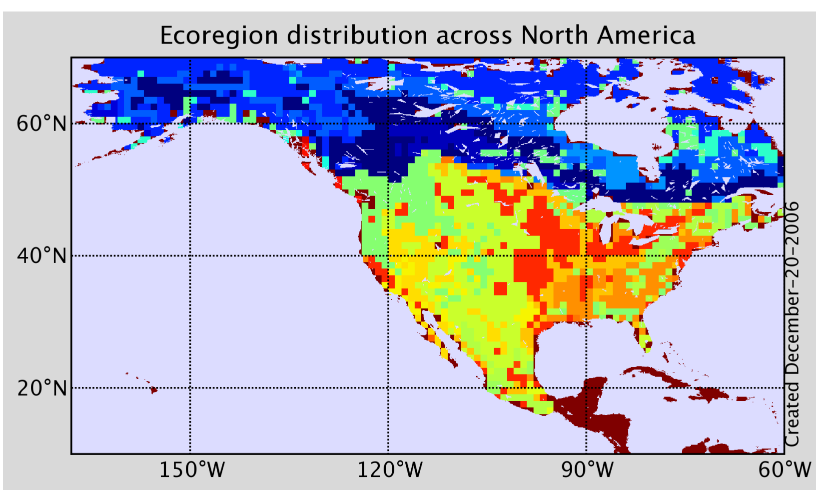

Theoretically, this approach leads to a total number of 11*19+30=239 optimizable scaling factors λ each week, but the actual number is 135 since not every ecosystem type is represented in each TransCom region, and because we decided not to optimize parameters for ice-covered regions, inland water bodies, and desert. The total flux coming out of these last regions is negligibly small. It is important to note that even though only one parameter is available to scale, for instance, the flux from coniferous forests in Boreal North America, each 1x1 degree grid box predominantly covered by coniferous forests will have a different flux F(x,y,t) depending on local temperature, radiation, and CASA modeled monthly mean flux.

Ecosystem types considered on 1x1 degree for the terrestrial flux inversions is based on Olson, [1992]. Note that we have adjusted the original 29 categories into only 19 regions. This was done mainly to fill the unused categories 16,17, and 18, and to group the from our perspective similar categories 23-26+29. The table below shows each vegetation category considered. Percentages indicate the area associated with each category for North America rounded to one decimal.

Ecosystem Types

category	Olson V 1.3a	Percentage area
1	Conifer Forest	19.0%
2	Broadleaf Forest	1.3%
3	Mixed Forest	7.5%
4	Grass/Shrub	12.6%
5	Tropical Forest	0.3%
6	Scrub/Woods	2.1%
7	Semitundra	19.4%
8	Fields/Woods/Savanna	4.9%
9	Northern Taiga	8.1%
10	Forest/Field	6.3%
11	Wetland	1.7%
12	Deserts	0.1%
13	Shrub/Tree/Suc	0.1%
14	Crops	9.7%
15	Conifer Snowy/Coastal	0.4%
16	Wooded tundra	1.7%
17	Mangrove	0.0%
18	Non-optimized areas (ice, polar desert, inland seas)	0.0%
19	Water	4.9%

Each 1x1 degree pixel of our domain was assigned one of the categories above bases on the Olson category that was most prevalent in the 0.5x0.5 degree underlying area.

2.2 Ensemble Size and Localization

The ensemble system used to solve for the scalar multiplication factors is similar to that in Peters et al. [2005] and based on the square root ensemble Kalman filter of Whitaker and Hamill, [2002]. We have restricted the length of the smoother window to only five weeks as we found the derived flux patterns within North America to be robustly resolved well within that time. We caution the CarbonTracker users that although the North American flux results were found to be robust after five weeks, regions of the world with less dense observational coverage (the tropics, Southern Hemisphere, and parts of Asia) are likely to be poorly observable even after more than a month of transport and therefore less robustly resolved. Although longer assimilation windows, or long prior covariance length-scales, could potentially help to constrain larger scale emission totals from such areas, we focus our analysis here on a region more directly constrained by real atmospheric observations.

Ensemble statistics are created from 150 ensemble members, each with their own background CO_2 concentration field to represent the time history (and thus covariances) of the filter. To dampen spurious noise due to the approximation of the covariance matrix, we apply localization [Houtekamer and Mitchell, 1998] for non-MBL sites only. This ensures that tall-tower observations within North America do not inform on for instance tropical African fluxes, unless a very robust signal is found. In contrast, MBL sites with a known large footprint and strong capacity to see integrated flux signals are not localized. Localization is based on the linear correlation coefficient between the 150 parameter deviations and 150 observation deviations for each parameter, with a cut-off at a 95% significance in a student's T-test with a two-tailed probability distribution.

2.3 Dynamical Model

In CarbonTracker, the dynamical model is applied to the mean parameter values λ as:

$$\lambda_t^b = (\lambda_{t-2}^a + \lambda_{t-1}^a + \lambda^p) / 3.0$$

Where "a" refers to analyzed quantities from previous steps, "b" refers to the background values for the new step, and "p" refers to real *a-priori* determined values that are fixed in time and chosen as part of the inversion set-up. Physically, this model describes that parameter values λ for a new time step are chosen as a combination between optimized values from the two previous time steps, and a fixed prior value. This operation is similar to the simple persistence forecast used in Peters et al. [2005], but represents a smoothing over three time steps thus dampening variations in the forecast of λ^b in time. The inclusion of the prior term λ^p acts as a regularization [Baker et al., 2006] and ensures that the parameters in our system will eventually revert back to predetermined prior values when there is no information coming from the observations. Note that our dynamical model equation does not include an error term on the dynamical model, for the simple reason that we don't know the error of this model. This is reflected in the treatment of covariance, which is always set to a prior covariance structure and not forecast with our dynamical model.

2.4 Covariance Structure

Prior values for λ^p are all 1.0 to yield fluxes that are unchanged from their values predicted in our modules. The prior covariance structure P^p describes the magnitude of the uncertainty on each parameter, plus their correlation in space. The latter is applied such that the same ecosystem types in different TransCom regions decrease exponentially with distance (L=2000km), and thus assumes a coupling *between* the behavior of the same ecosystems in close proximity to one another (such as coniferous forests in Boreal and Temperate North America). Furthermore, all ecosystems *within* tropical TransCom regions are coupled decreasing exponentially with distance since we do not believe the current observing network can constrain tropical fluxes on sub-continental scales, and want to prevent large dipoles to occur in the tropics.

In our standard assimilation, the chosen standard deviation is 80% on land parameters, and 40% on ocean parameters. This reflects more prior confidence in the ocean fluxes than in terrestrial fluxes, as is assumed often in inversion studies and partly reflects the lower variability and larger homogeneity of the ocean fluxes. All parameters have the same variance within the land or ocean domain. Because the parameters multiply the net-flux though, ecosystems with larger weekly mean net fluxes have a larger variance in absolute flux magnitude.

3. Further Reading

- Whitaker and Hamill, 2002 paper
- Peters et al., 2005 paper
- Olson ecosystem types, data